Proceedings of the Institute of Acoustics

FEM ANALYSIS OF SONAR TRANSDUCERS

S.S.Jarng, B.V.Smith and J.R.Dunn

School of Electronic & Electrical Engineering
University of Birmingham
Birmingham B15 2TT

1 INTRODUCTION

SONAR transducers [1,2,3] are used for radiating and receiving underwater sound waves in SONAR systems. Different types of transducer are used depending on the application. There are many transducer design factors which need to be considered in relation to the overall design of the SONAR system. Magnetostrictive and piezoelectric transducers are limited to simple shapes, whereas electrostrictive ceramic materials, such as barium titanate ($BaTiO_3$) or lead zirconate titanate (PZT), can be readily moulded into desirable forms and so are almost exclusively used in underwater acoustic applications.

It is clearly necessary to develop models of the transducers so that the designer is able to meet specifications. These models are inherently either analytical or numerical in character. The main advantage of numerical methods, such as the finite-element method (FEM), over analytical methods, such as equivalent circuit modelling, is that truly 3-dimensional dynamics can be properly studied. The main aim of this paper is to outline the development and validation of a piezoelectric "brick" finite-element as part of a program to develop software for SONAR transducer design.

2 EXPERIMENTAL RESULTS

Let us first consider the steady-state frequency response of two simple SONAR transducers made of PZT4; a bar and a ring. These have been studied in order to easily compare theoretical results with experimental results. Fig.1(a) shows the admittances of the bar transducer for different frequencies from zero Hz to 60 KHz. The magnitudes of the admittances were measured in air by an impedance analyzer (HP model 4192A LF). The x-axes (frequency axes) are linear while the y-axes are expressed on a log scale. Fig.1(b) shows the magnitudes of the admittance response in greater detail around the fundamental resonant frequency (f_o). The Q-factor of the bar transducer in air is about 623. It should be noted that the ratio of the third and the fundamental resonant frequencies ($f_3 \div f_o$) is about 2.91. Fig.2 shows the admittances of the ring transducer. The Q-factor of the ring transducer in air is about 667.

3 SONAR TRANSDUCER MODELLING

The basis of the linear modelling of a SONAR transducer is the piezoelectric equations ,i.e. a pair of coupled electro-elastic equations which govern the effects of the piezoelectricity.

For the stress $[\sigma] = [C][e] - [e_p][E]$ (1a)

For the charge density $[q] = [e_p]^t[e] + [\epsilon][E]$ (1b)

where brackets represent matrices, and the superscript t represents the transpose of the matrix. The coefficients may be arranged in a 9x9 symmetric matrix.

The electric circuits representing the transducer characteristics are limited to one-dimensional applications. Details of the equivalent circuits and their components are given by D.A.Berlincourt et. al. [4].

FEM has proved to be a powerful numerical technique for solving problems in which the electric field couples to the mechanical stress and strain [5,6,7]. It has flexibility in that it can be used to model any arbitrary geometry and characterize any given property of material. The effects of structural damping and fluid radiation can be progressively added to the primary computational program.

Three approximations are applied to the FEM and the accuracy of the numerical solution depends on the degree of each approximation. Firstly, the bounded domain of a given structure is divided up into a finite number of smaller elements. Each element is specified by a discrete number of nodes within the element or on its perimeter. Secondly, the variable in the piezoelectric equations at a point within an element or on its boundary is approximated throughout the element by interpolation between the nodal values [8]. The functions of a co-ordinate system which define the interpolation are called element shape functions. Thirdly, the volume integration of the piezoelectric equations is implemented numerically for each element by means of the Gauss-Quadrature approximation [10]. 20 nodes for each hexahedral element have been isoparametrically interpolated by the parabolic shape function of the Serendipity family [9]. As the whole bounded domain is reduced into subelements of a far smaller size, and as the elemental integration of the piezoelectric equations is accomplished with a larger number of Gauss points, the results of the FEM solution for the piezoelectric equations become more accurate.

The finite element equations for the dynamic piezoelectric structural system are given by

$$[F_A] = [K_{uu}][a] + [K_{u\phi}][\phi] - \omega^2[M][a] + j\omega[R][a] \quad (2a)$$

$$-[Q] = [K_{\phi u}][a] + [K_{\phi\phi}][\phi] \quad (2b)$$

where $[F_A]$ represents externally driven forces, $[Q]$ represents externally driven charges, and $[a]$ represents nodal displacements, $[\phi]$ represents nodal electric potentials. The element matrices of $[K_{uu}]$, $[K_{u\phi}]$, $[K_{\phi u}]$, $[K_{\phi\phi}]$, $[M]$, $[R]$ are defined to be elastic stiffness matrix, piezoelectric stiffness matrix, inverse piezoelectric stiffness matrix, dielectric stiffness matrix, mass matrix and

dissipation matrix respectively. Material data for each element is represented by the element matrices. Details of isoparametric derivation of element matrices are presented by H.Allik et. al. [6].

A note should be added concerning elements near the boundary which are subject to a constant pressure drive. If only a plane pressure is considered, the external pressure should be distributed into each node on the boundary surface in terms of nodal forces. A nodal force normal to the boundary surface is derived by surface integration [10,11]:

$$F^i = \int_{A^e} N^i \bar{p} dS$$

where N^i is the shape function of the corresponding node, A^e is the force-driven boundary and $\bar{p}$ is the constant external pressure on A^e. For the parabolic shape function of the Serendipity family, the typical ratio between the normal forces on the corner node and on the midside node is -1:4. The nodal forces overlapped by adjacent elements are simply summed.

All the element matrices over the whole domain are systematically combined into global matrices and the assembled global equation is solved to evaluate the set of unknown nodal values (e.g. displacement vector and potential scalar). The assembly of the system matrices requires consistent node or element ordering. The equilibrium conditions are modified according to the prescribed boundary conditions [12]. That is, the equivalent representation of an equipotential surface need the transformation of the assembled global coefficient matrix. It is done by adding all affected rows and columns to the one row and column selected to represent the equipotential surface and then deleting them from the global matrix. Also, another transformation of the assembled coefficient matrix is associated with the representation of clamped boundary conditions. This is done by deleting all affected rows and columns from the global matrix since the displacement normal to the clamped boundary is assumed to be zero. The second matrix transformation is particularly useful for the FEM modelling with geometric symmetry. Gauss-elimination technique or Gauss-reduction technique [13] are used for solving the assembled equation of system matrices. Use of the element shape functions together with these nodal values then enables the unknown physical variables to be determined throughout the whole domain.

4 RESULTS AND DISCUSSION

It is difficult in practice to measure all the three-dimensional material parameters of PZT4 (coefficients in equation 1). Since the measured parameters from the experimental transducer models are insufficient for the three-dimensional FEM models, the manufacturer's properties for PZT4 ceramics have been used for the theoretical models (refer [4]).

Fig.3 compares the measured frequency response for the bar transducer (thick lines) with that of the FEM bar model (thin lines). The mechanical damping, Rm, of the bar model is 7.6 kg/sec which produces a Q-factor of about 618 in air. It should be also noted that the ratio of the third and the fundamental resonant frequencies is about 2.925. This numerical ratio is very similar to the experimental ratio in Fig.1. A similar set of results have been obtained for the ring transducer. The Q-factor of the ring model in air is about 674 with Rm=2.0 Kg/sec. The value of Rm was arbitrarily changed to produce an approximate Q-factor similar to the experimental Q-factor.

In the same way, Fig.4 compares the measured frequency response for the bar transducer (thick lines) with the analytical bar model (thin lines). The analytical model produces the same Q-factor as the FEM model with Rm=7.6 Kg/sec. The ratio of the third and the fundamental resonant frequencies is 3.0. Again similar results are obtained with ring transducer. The analytical model produces the same Q-factor as the FEM model with Rm=2.0 Kg/sec.

These results, Fig.3 and 4, show that both the numerical and analytical models predict results which are in quite good agreement with experimental measurements even though the manufacturer's properties of PZT4 ceramics have been used for the models. However, the ratios of the third and fundamental resonant frequencies from the experimental measurements and the FEM results are smaller than 3 (2.91 and 2.925 respectively). This is because of structural aspect ratio, which can be demonstrated by decreasing the cross-section of the model structure. That is, the analytical and the FEM results of the same bar model become very close when the aspect ratio of the FEM model is reduced (see Fig.5). Fig.5 shows the admittance responses of the FEM bar model (thick lines) and the analytical bar model (thin lines). In Fig.5(a), the structure of both models is the same as the previous case, whereas in Fig.5(b) the cross-section of both models have been reduced. Therefore as anticipated the three-dimensional FEM approach for the SONAR transducer modelling gives results which are in better agreement with the measurements than does the one-dimensional analytical approach.

The FEM bar and ring models also enable the strains to be observed by generating diagrams of the relevant geometry showing the deformations. Examples of these will be shown during the presentation.

Finally, the effects of solid-fluid interfacing can be added to the primary structural finite element program. Let us briefly consider the radiation effects in an infinite fluid domain. Fig.6 shows the difference of the frequency response of the admittance between an in-air ring transducer model (thin line) and an under-water ring transducer model (thick line). Fig.6(a) and (b) show the magnitudes and the phases of the admittances. In general, the main effects of fluid loading on the structure are to introduce fluid damping and increase the inertia of the structure, therefore lowering the resonant frequencies [15]. Details of acoustic radiation formulation for a coupled finite element-boundary integral may be found in reference [16]. Essentially, the mathematical expression for the solid-fluid interfacing is incorporated by simply adding an extra equation, $[F_f]$, to equation 2a and equation 2b.

$$[F_I] + [F_A] = [K_{uu}][a] + [K_{u\phi}][\phi] - \omega^2[M][a] + j\omega[R][a] \quad (3a)$$

$$-[Q] = [K_{\phi u}][a] + [K_{\phi\phi}][\phi] \quad (3b)$$

where $[F_I]$ represents the interaction forces generated by the acoustic fluid acting on the fluid-solid boundary. The interaction force vector can be defined through a coupling matrix $[L]$ and a fluid impedance matrix $[K_f]$, that is,

$$[F_I] = \omega^2\rho_f[L][K_f]^{-1}[L]^t[a] \quad (4)$$

where ρ_f is fluid density.

5 REFERENCES

[1] Urick R.J. (1983): Principles of underwater sound, 3rd edition, McGraw-Hill, New York, London.

[2] Gazey B. K., McQueen P. D. and Smith B.V. (1989): Lecture notes for post-experience course on underwater acoustics and sonar systems, School of Electronic and Electrical Engineering, University of Birmingham.

[3] Design and construction of crystal transducers, design and construction of magnetostrictive transducers, Nat. Def. Res. Comm. Div. 6 Sum. Tech. Reps. 12 and 13, 1946.

[4] Berlincourt D.A., Curran D.R. and Jaffe H. (1964): Piezoelectric and piezomagnetic materials and their function in transducers, Physical acoustics: Principles and methods edited by W.P. Mason, Academic Press, vol. 1, part A, chapter 3, pp:169-269.

[5] Allik H. and Hughes T.J.R (1970): Finite element method for piezoelectric vibration, Int. J. Numer. Method. Eng., vol. 2, pp:151-157.

[6] Allik H., Webman K.M. and Hunt J.T. (1974): Vibrational response of sonar transducers using piezoelectric finite elements, J. Acoust. Soc. Am., vol. 56, no. 6, pp:1782-1791.

[7] Kagawa Y. and Yamabuchi T. (1976): Finite element approach for a piezoelectric circular rod, IEEE Trans. Sonics & Ultrasonics, Vol. su-23, No. 6, pp:379-385.

[8] Smith B.V. (1988): Finite element principles, Proc. Inst. of Acoust., vol. 10, part 9, pp:16-37.

[9] Cheung Y.K. and Yeo M.F. (1979): A practical introduction to finite element analysis, Pitman publishing Ltd., London.

[10] Zienkiewicz O.C. (1977): The finite element method, 3rd edition, McGraw-Hill, London, pp:178-210.[PB]

[11] Brebbia C.A. and Ferrante A.J. (1978): Computational methods for the solution of engineering problems, 2nd edition, Pentech press, London:Plymouth.

[12] Hardie D.J.W. (1988): Introduction to finite elements, Proc. Inst. of Acoust., vol. 10, part 9, pp:1-15.

[13] Dunn J.R. (1988): The structure of a simple program, Proc. Inst. of Acoust., vol. 10, part 9, pp:38-46.

[14] McDearmon G.F. (1984): The addition of piezoelectric properties to structural finite element programs by matrix manipulations, J. Acoust. Soc. Am., vol. 76(3), pp:666-669.
[15] Macey P.C. (1988): Fluid loading and piezoelectric elements, Proc. Inst. of Acoust., vol. 10, part 9, pp:79-104.
[16] Mathews I.C. (1986): Numerical techniques for three-dimensional steady-state fluid-structure interaction, J. Acoust. Soc. Am., vol. 79(5), pp:1317-1325.

********** ********** **********

Figures

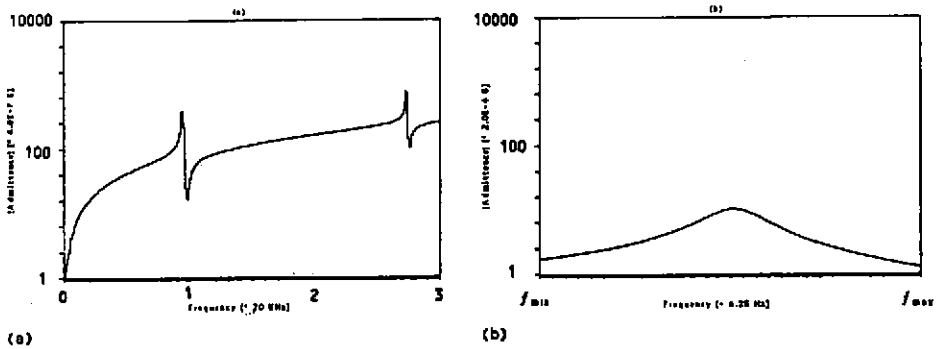

Fig.1 Measured admittance responses of a bar SONAR transducer in air
(a) |Admittance| [* 6.0E-7 S] vs Frequency [* 20 KHz]
(b) |Admittance| [* 2.0E-4 S] vs Frequency [* 6.25 Hz]
The interval of each division in (b) is 6.25 Hz.
f_{min} = 18.61075*KHz* , f_s = 18.7*KHz* , f_1 = 54.5*KHz* , f_{max} = 18.79825*KHz*

FEM ANALYSIS OF SONAR TRANSDUCERS

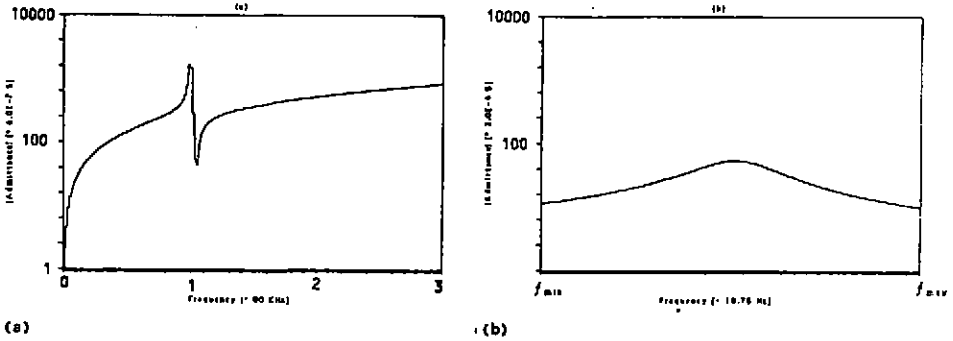

(a) (b)

Fig.2 Measured admittance responses of a ring SONAR transducer in air
(a) |Admittance| [* 6.0E-7 S] vs Frequency [* 80 KHz]
(b) |Admittance| [* 2.0E-4 S] vs Frequency [+ 18.75 Hz]
f_{min}=78.49575KHz . f_s=78.8KHz . f_{max}=79.05825KHz

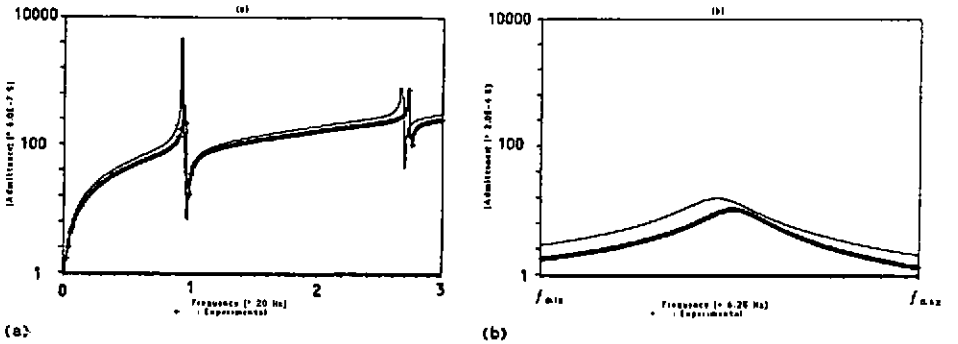

(a) (b)

Fig.3 Admittance responses of a bar transducer measured (thick lines) and a FEM bar model (thin lines) in air
(a) |Admittance| [* 6.0E-7 S] vs Frequency [* 20 KHz]
(b) |Admittance| [* 2.0E-4 S] vs Frequency [+ 6.25 Hz]
Exp. (*thick lines*) : f_{min}=18.61075KHz . f_s=18.7045KHz . f_{max}=18.79825KHz
FEM (thin lines) : f_{min}=18.14625KHz . f_s=18.2400KHz . f_{max}=18.33375KHz

FEM ANALYSIS OF SONAR TRANSDUCERS

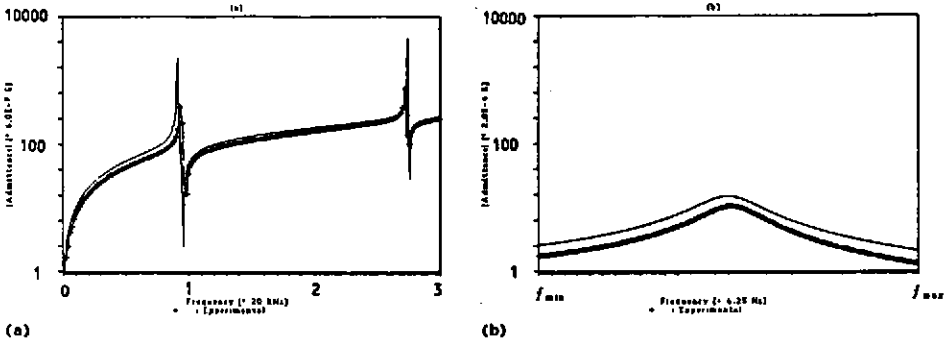

Fig.4 Admittance responses of a bar transducer measured (thick lines) and an analytical bar model (thin lines) in air
(a) |Admittance| [* 6.0E-7 S] vs Frequency [* 20 KHz]
(b) |Admittance| [* 2.0E-4 S] vs Frequency [+ 6.25 Hz]
Exp. (*thick lines*) : f_{min} = 18.61075*KHz* . f_r = 18.70450*KHz* . f_{max} = 18.79825*KHz*
Ant. (*thin lines*) : f_{min} = 18.19754*KHz* . f_r = 18.29129*KHz* . f_{max} = 18.38504*KHz*

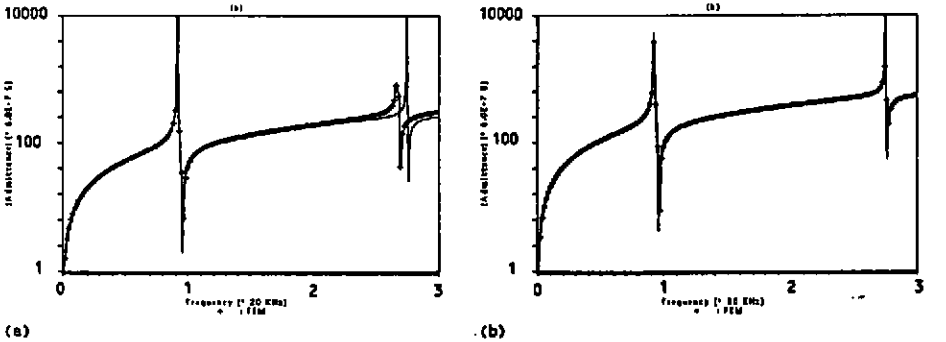

Fig.5 Admittance responses of a FEM bar model (thick lines) and an analytical bar model (thin lines) in air
length of the bar model is the same in (a) and (b), but the cross-section of the bar was reduced in (b).
(a),(b) |Admittance| [* 6.0E-7 S] vs Frequency [* 20 KHz]

FEM ANALYSIS OF SONAR TRANSDUCERS

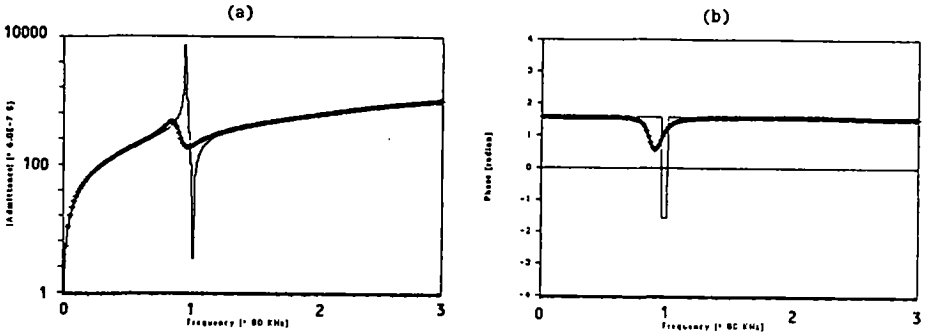

Fig.6 Admittance responses of a FEM ring model in air (thick lines) and a FEM ring model in infinite water domain (thin lines) Rm=7.6 Kg/sec
(a) |Admittance| [* 6.0E-7 S] vs Frequency [* 80 KHz]
(b) Phase [radian] vs Frequency [* 80 KHz]